Supporting Information

Denatured bovine serum albumin particle decorated graphene oxide nanocomposite for ultrasensitive resistive humidity sensing

Pan Qi, Yongkang Zhang, Ziang Zhang, Xiaobing Li, and Cunlan Guo*

College of Chemistry and Molecular Sciences, Wuhan University, 299 Bayi Road, Wuhan, Hubei 430072, China

E-mail: cunlanguo@whu.edu.cn

1. Preparation and characterizations

1.1 Preparation

1.1.1 Template-stripped Au substrate (Au^{TS})

The Si wafer was cleaned by sonication with deionized water, acetone, and isopropyl alcohol for 5 min in turn. Then, it was further treated with plasma for 3 min under a mixture of O_2 and Ar in equal proportions, and etched with 2% HF. The plasma treatment and HF etching were repeated again. Finally, the SiO_2 layer was grown by plasma treatment for 10 min under O_2 atmosphere. A 100 nm Au was evaporated on the cleaned Si wafers at a gradually accelerating rate by a thermal evaporator (JSD-300, Jiashuo Technology Co., Ltd). About 0.6 cm^2 of glass were glued to the Au-plated Si wafer by ultraviolet adhesive (Norland, No. 61), which was illuminated with ultraviolet lamps for 4 h to cure the glue. The glass can completely strip the Au layer from the Si wafer to get a fresh and clean Au surface.

1.1.2 Self-assembled monolayer of BSA on Au^{TS} substrate

First, the fresh Au^{TS} substrate was immersed in 2-MEA aqueous solution (0.065 M) and cleaned with deionized water after 1 h. Next, the BSA aqueous solution (1 mg/mL) was dropped on the Au^{TS} substrate assembled with linker 2-MEA and was rinsed with deionized water after 4 h at 4℃.

1.1.3 Denatured BSA particle (dBSA) nanofilm assembling on Au^{TS} substrate

The dBSA solution was a mixture of 50 mM TCEP aqueous solution and 2 mg/mL BSA aqueous solution at a volume ratio of 1:1. The pH of TCEP solution was adjusted to 5.0 by 5 M NaOH. The dBSA nanofilm can be obtained by incubating Au^{TS} slide in fresh dBSA solution at 4 ℃ for a period of time and rinsing the slide with water. Proper extension time can obtain different thickness of dBSA nanofilm.

1.1.4 GO nanofilm on Au^{TS} substrate

The GO (0.3 mg/mL) was suspended in water by ultrasonication for 2 h and the suspension was centrifuged (4000 rpm, 15 ℃) for 15 min to remove large particles. Multilayer GO nanofilm was fabricated by drop-casting, in which about 50 μL of supernatant was dropped on the Au^{TS} substrate and dried at 30 ℃ or by N_2 stream.

1.1.5 dBSA-GO hybrid nanofilm on Au^{TS} substrate

After 2 h sonication and centrifugation of GO as well as 1 h reaction of BSA and TCEP, 10 times volume of GO supernatant was added to dBSA solution. After another 20 min sonication, the mixture was dropped on the Au^{TS} substrate and dried at 30 °C. Besides, a dBSA/GO nanofilm stacked layer by layer was also prepared as a control. dBSA was first assembled on Au^{TS} substrate and then the GO nanofilm.

1.2 Characterizations

1.2.1 Ellipsometry measurement

The thicknesses of BSA monolayer and dBSA nanofilm were measured by a J.A. Woollam M-2000 spectroscopic ellipsometer. The values at incident angles of 65°, 70°, and 75° were collected and fitted to get the average results. For data fitting, the bare gold substrate (Au^{TS}) was first fitted similar to bulk material to get the refractive index (n) and extinction coefficient (k). Then, the nanofilm on Au^{TS} was fitted using the Cauchy model, assuming n is equal to 1.5.

1.2.2 Atomic force microscopy (AFM)

The morphologies of nanofilms were examined by a Park NX10 AFM with a Si cantilever (HQ: XCS11/Al tip from MikroMasch, spring constant ~2 N/m, resonance frequency ~80 kHz, sensitivity ~45 V/μm) in tapping mode. 256 points per row at a scan rate of 1 Hz were applied for morphology imaging. The films with partial scratching were further imaged to obtain the film thickness.

The shifts in work function with relative humidity (RH) for dBSA or dBSA-GO modified Au^{TS} substrates were analyzed with Kelvin probe, which was performed by a Park NX10 AFM in EFM mode. The AFM tip for Kelvin probe measurements was from MikroMasch (HQ: XSC11/Pt, spring constant ~7 N/m, resonance frequency ~155 kHz). Highly-ordered pyrolytic graphite (HOPG) was placed in the same environmental chamber for calibration by the following formula:

$$WF_{tip} - V_{CPD} = WF_{sample} \#(1)$$

where V_{CPD} is the potential difference between the sample and the tip. It is generally considered that the work function of HOPG has negligible changes in the same ranges of RH.

1.2.3 Polarization modulation-infrared reflection-absorption spectroscopy (PM-IRRAS)

Infrared spectra of the nanofilms modified Au^{TS} surfaces were obtained by a Bruker INVENIO R Fourier transform infrared spectrometer with a photoelastic modulator (PEM-100, Hinds Instruments) and a liquid N_2-cooled mercury cadmium telluride (MCT) detector. All spectra (400−6000 cm^{-1}) were recorded at an incident angle of 85° with the modulation centered at 1600 cm^{-1}. For each sample, 2000 scans were recorded at a resolution of 2 cm^{-1}.

1.2.4 Water contact angles

The contact angles of the nanofilms were measured by a POWEREACH® JC2000C contact angle measuring instrument. A droplet of the water (5 μL) was dropped onto the nanofilms for measurements. Images of the droplets on the nanofilms were analyzed with the POWEREACH® software.

1.2.5 Circular dichroism (CD)

CD spectra were collected using a Jasco-810 spectropolarimeter (Jasco, Easton, MD, USA) under constant N_2 flush at 25°C and recorded from 185 nm to 260 nm with a 1.0 nm bandwidth. All CD spectra were baseline-corrected with deionized water as background and were averaged from three runs. The prepared dBSA solution was diluted for CD measurements.

1.2.6 Fluorescence spectra of ThT and ANS

After 6 h incubation at 4 ℃, the dBSA solution was mixed with the 10 mM aqueous solution of ThT or ANS at a volume ratio of 50:1 for 1 h in the dark. The samples were measured by RF-6000 fluorescence spectrophotometer (Shimadzu) with 5 nm slits for excitation and emission. The excitation wavelength of ANS and ThT was 398 and 440 nm, respectively. The emission spectrum was from 300 to 700 nm for ANS and from 400 to 800 nm for ThT with a step of 0.2 nm.

1.2.7 UV-visible spectra

Ellman's reagent, also known as DTNB, is a water-soluble compound. The DTNB can be reduced to TNB via breaking the disulfide bond by the free thiol groups in peptides and proteins. The absorption of TNB at 412 nm was applied to quantify the content of

free thiol groups in peptides and proteins. After 6 h incubation at 4 ℃, the dBSA solution was mixed with 1 mM DTNB solution at a volume ratio of 1:1. The mixed solution was tested directly by UV-visible spectroscopy (Nanodrop One, Thermo Scientific) from 190 to 850 nm.

References

[1] Y. Pang, J. Jian, T. Tu, Z. Yang, J. Ling, Y. Li, X. Wang, Y. Qiao, H. Tian, Y. Yang and T.-L. Ren, *Biosens. Bioelectron.* 2018, **116**, 123–129.

[2] S.J. Choi, H. Yu, J.S. Jang, M.H. Kim, S.J. Kim, H.S. Jeong and I.D. Kim, *Small* 2018, **14**, 1703934.

[3] S. Borini, R. White, D. Wei, M. Astley, S. Haque, E. Spigone, N. Harris, J. Kivioja and T. Ryhänen, *ACS Nano* 2013, **7**, 11166–11173.

[4] D. Tripathi, S. Tripathi, R.K. Rawat and P. Chauhan, *J. Electron. Mater.* 2023, **52**, 2396–2408.

[5] Y. Jiang, J. Ma, L. Shen, W. Zhang, K. Yang, B. Zhu, Y. Yang, H. Ma, X. Chen, S. Bai and N. Zhu, *ACS Appl. Mater. Interfaces* 2023, **15**, 47196-47207.

[6] M. Sasmal, S. Majumder and T.K. Bhattacharyya, *IEEE Sens. J.* 2018, **18**, 8223–8229.

[7] M. Sasmal, T.K. Maiti and T.K. Bhattacharyya, *IEEE Sens. J.* 2016, **16**, 1510–1517.

[8] L. Lan, X. Le, H. Dong, J. Xie, Y. Ying and J. Ping, *Biosens. Bioelectron.* 2020, **165**, 112360.

[9] C. Zhu, L.-Q. Tao, Y. Wang, K. Zheng, J. Yu, X. L, X. Chen and Y. Huang, *Sens. Actuator B-Chem.* 2020, **325**, 128790.

[10] F.J. Romero, A. Rivadeneyra, M. Becherer, D.P. Morales and N. Rodriguez, *Micromachines* 2020, **11**.

[11] Z. Wu, X. Sun, X. Guo, Y. Ding, Y. Ou, H. Yang, Y. Chen, Y. Hu, D. Kuang, C. Zhao and Y. He, *ACS Appl. Mater. Interfaces* 2021, **13**, 27188–27199.

[12] H. Cheng, Y. Huang, L. Qu, Q. Cheng, G. Shi and L. Jiang, *Nano Energy* 2018, **45**, 37–43.

[13] B.A. Boukamp, *J. Electrochem. Soc.* 1995, **142**, 1885-1894.

[14] M. Schönleber, D. Klotz and E. Ivers-Tiffée, *Electrochim. Acta* 2014, **131**, 20-27.

[15] T.H. Wan, M. Saccoccio, C. Chen and F. Ciucci, *Electrochim. Acta* 2015, **184**, 483–499.

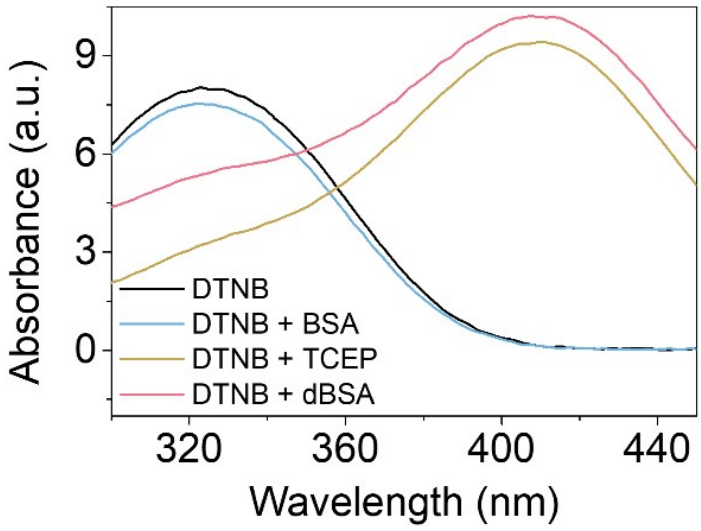

Figure S1. UV-visible spectra of DTNB with and without BSA, TCEP, and dBSA solution.

Since both TCEP and the thiol group of dBSA have the ability to break the DTNB disulfide bond and generate TNB, DTNB+TCEP and DTNB+dBSA were specifically compared here. For DTNB+dBSA, TCEP was first mixed and reacted with BSA, and the remained TCEP could react with DTNB. In contrast, DTNB+dBSA showed a higher UV absorption than DTNB+TCEP, indicating that dBSA did exist in solution and reacted with DTNB.

Table S1. Thickness of BSA monolayer and dBSA nanofilms by Ellipsometry.

	2-MEA	BSA	dBSA 4.5 h	dBSA 8 h	dBSA 13 h	dBSA 15 h
Thickness (nm)	0.5 ± 0.1	3.1 ± 0.1	10.8 ± 1.5	20.1 ± 2.6	34.3 ± 2.7	38.5 ± 0.8

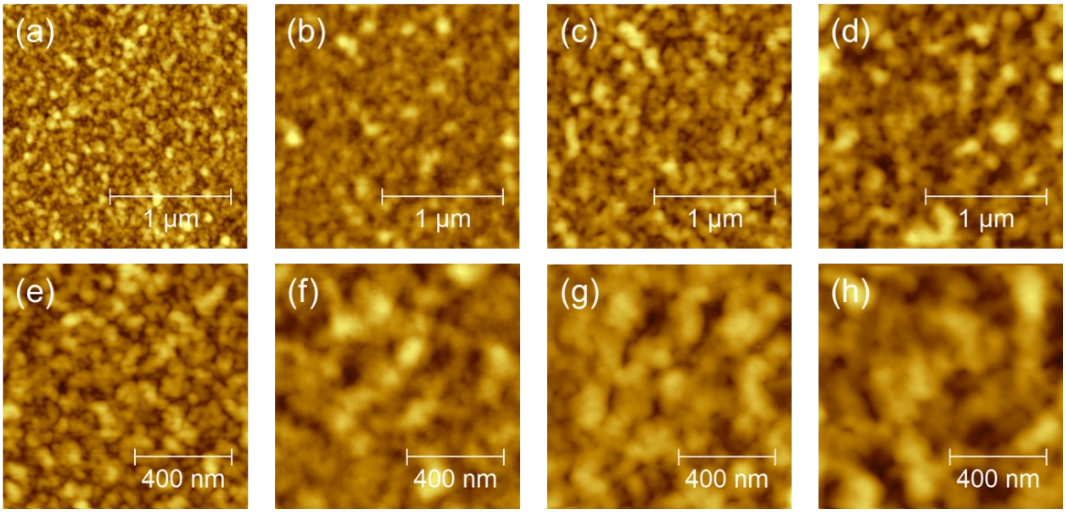

Figure S2. AFM images of dBSA nanofilms with thicknesses of (a, e) 11 nm, (b, f) 20 nm, (c, g) 34 nm, and (d, h) 39 nm made by controlling incubation time for 4.5, 8, 13, and 15 hours.

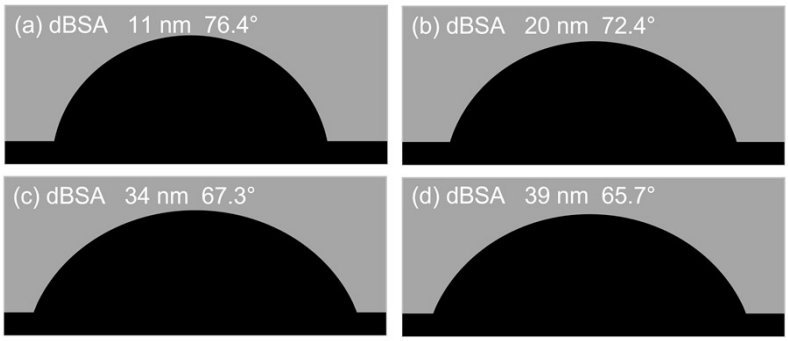

Figure S3. Water contact angle of dBSA nanofilms with thicknesses of (a) 11 nm, (b) 20 nm, (c) 34 nm, and (d) 39 nm.

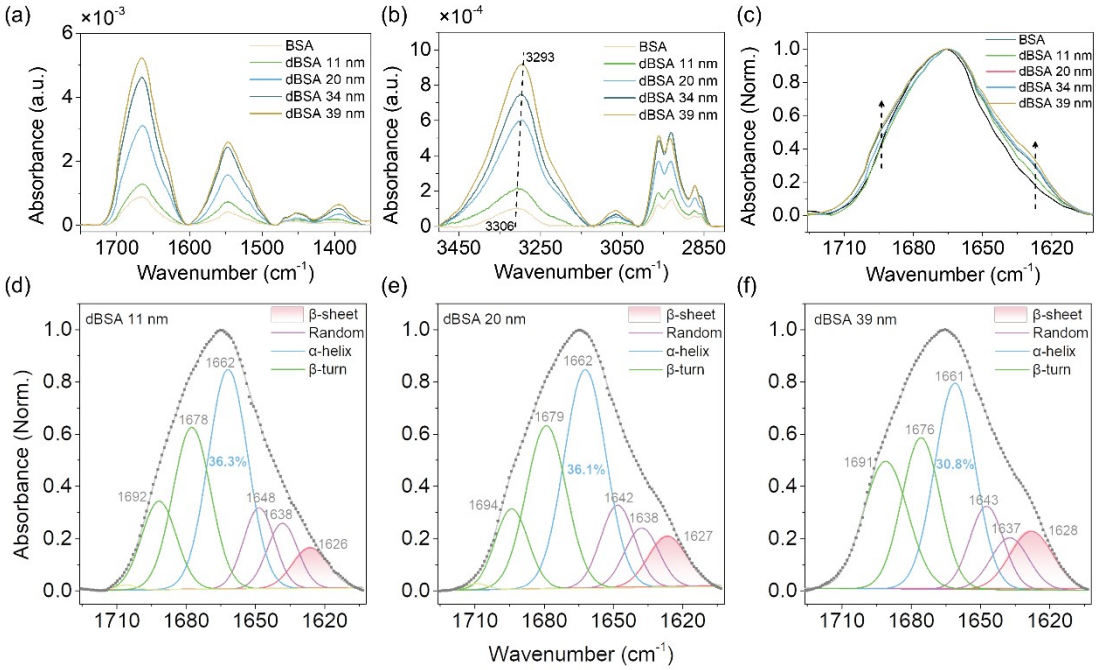

Figure S4. PM-IRRAS spectra of BSA monolayer and dBSA nanofilms in (a) 1750–1350 cm^{-1}, (b) 3500–2800 cm^{-1} regions, and (c) amide I range. Deconvolution and Gaussian peak fitting for the amide I band of (d) dBSA-11 nm nanofilm, (e) dBSA-20 nm nanofilm, and (f) dBSA-39 nm nanofilm.

The denaturation degrees were analyzed from PM-IRRAS results. As shown in Figure S4a-S4b), the intensity of the infrared absorption peaks around 1600 cm^{-1} and 3000 cm^{-1} significantly increased with the incubation time and dBSA oligomer size, which may be attributed to the increased number of molecules within the nanofilms. In addition to the changes in intensity, there were also apparent alterations in peak shape. For instance, the peak representing the O-H stretching vibration associated with hydrogen bonding gradually broadened and red-shifted from 3306 cm^{-1} to 3293 cm^{-1}, indicating an increase in the number of hydrogen bonds. In Figure S4c, the normalized amide I band were in the range of 1687–1650 cm^{-1}. However, the shoulder peak at 1627 cm^{-1} gradually intensified, and the shoulder at 1692 cm^{-1} also increased with large size of dBSA. Deconvolution and peak fitting of the amide I band indicated the decrease in α-helix content as well as increases in β-sheet and β-turn content (Figure S4d-S4f).

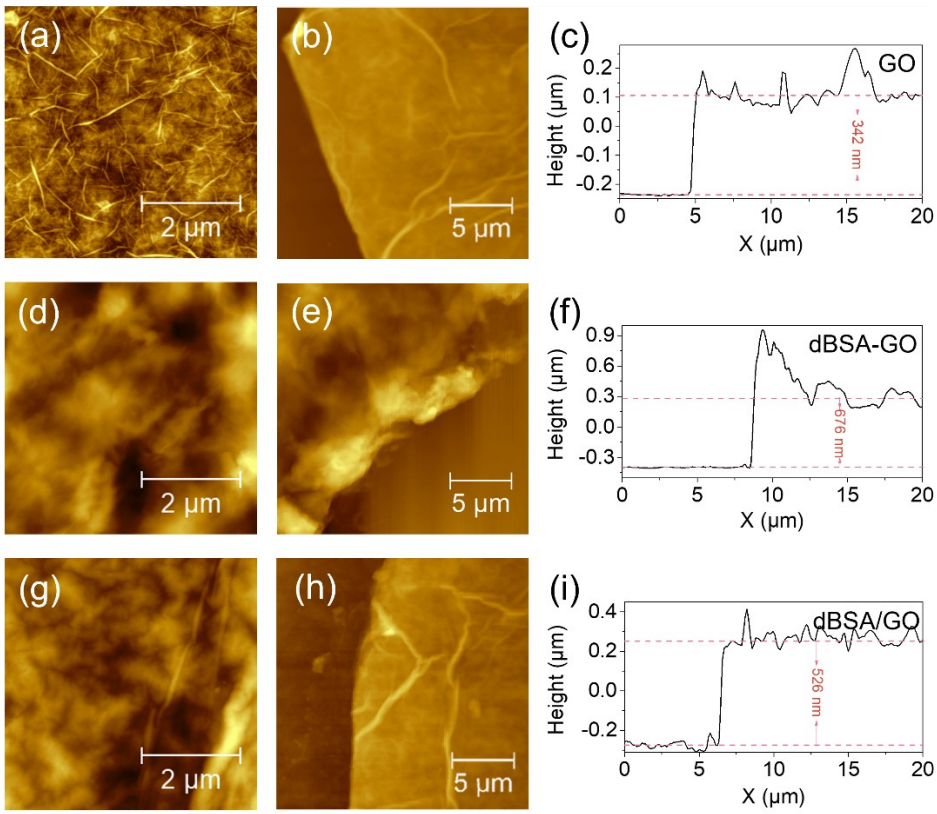

Figure S5. AFM morphologies and height profiles of (a-c) GO, (d-f) dBSA-GO, and (g-i) dBSA/GO nanofilms. The height profiles were obtained by imaging the locations after scratching.

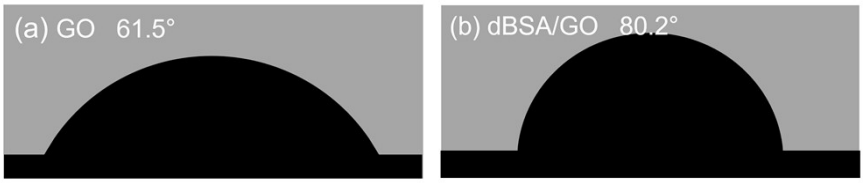

Figure S6. Water contact angle of (a) GO nanofilm and (b) dBSA/GO nanofilm.

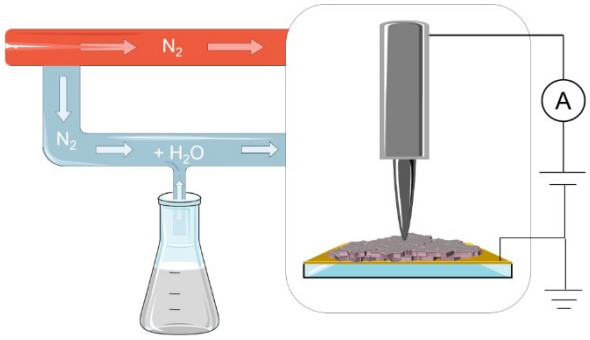

Figure S7. Schematic diagram of the humidity sensor testing setup.

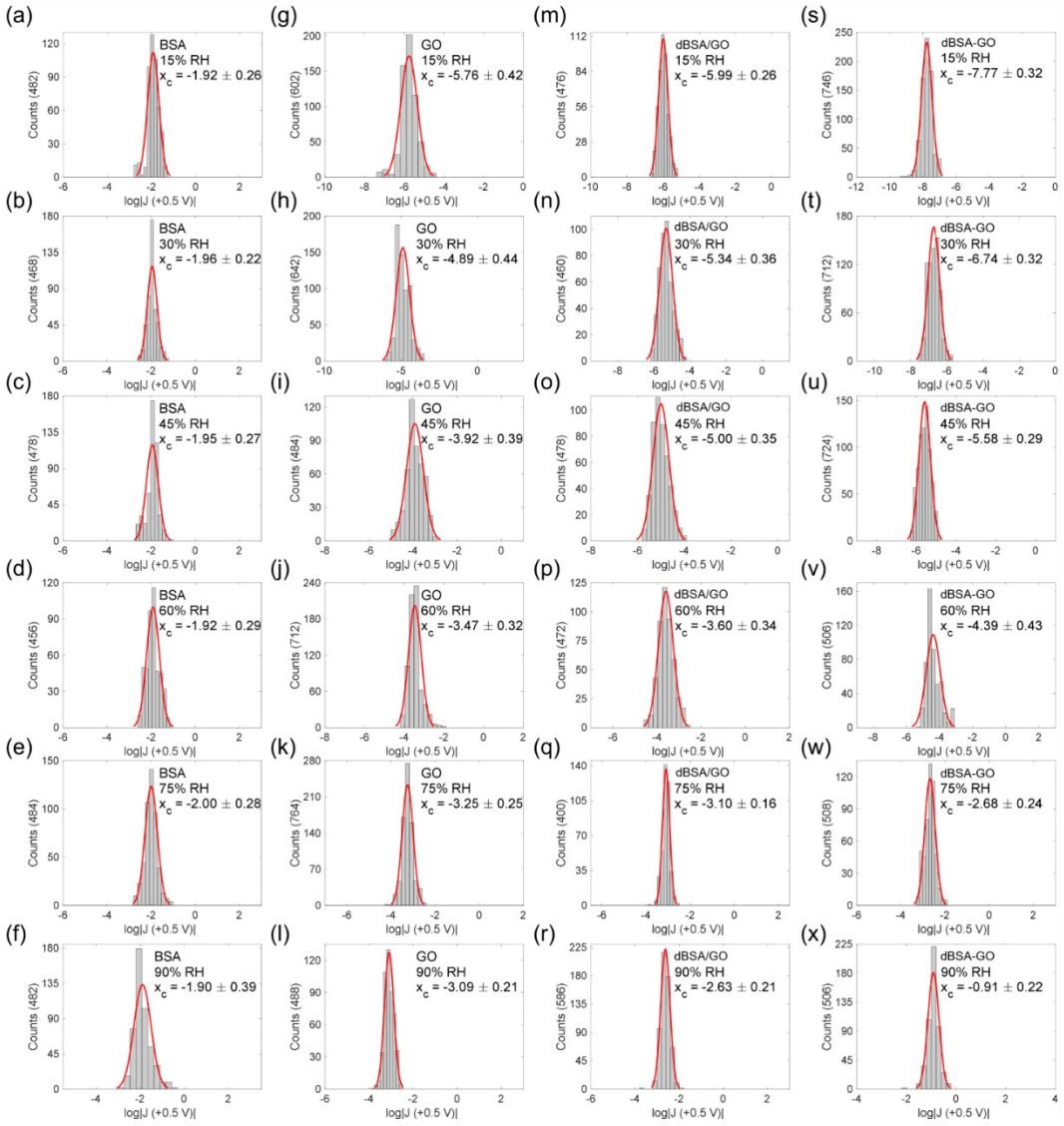

Figure S8. Histograms of current density at +0.5 V for (a-f) BSA monolayer junction, (g-l) GO nanofilm junction, (m-r) dBSA/GO nanofilm junction, and (s-x) dBSA-GO nanofilm junction under RH from 15% to 90% with 15% intervals.

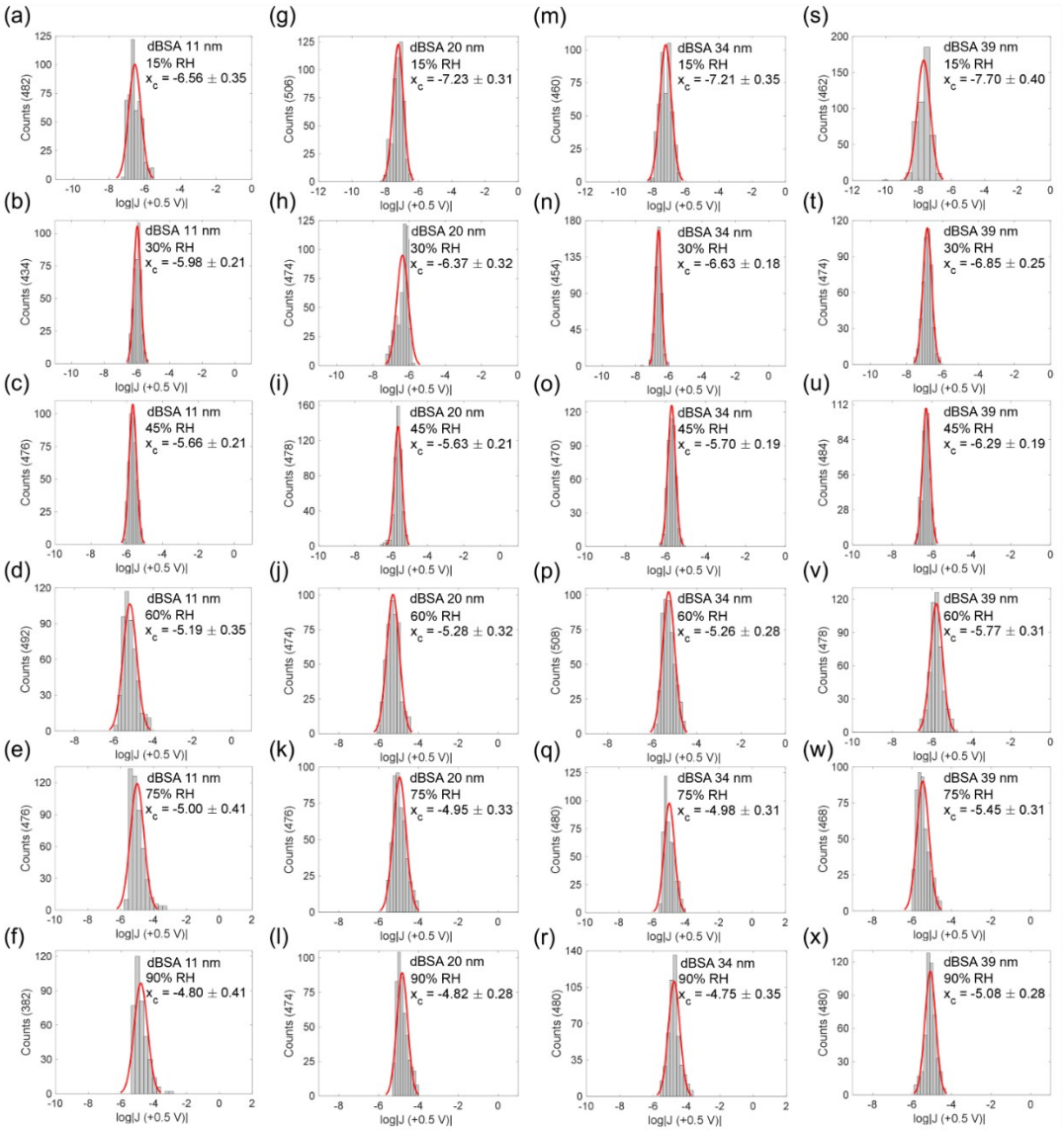

Figure S9. Histograms of current density at +0.5 V for dBSA nanofilm junctions with dBSA thickness of (a-f) 11 nm, (g-l) 20 nm, (m-r) 34 nm, and (s-x) 39 nm under RH from 15% to 90% with 15% intervals.

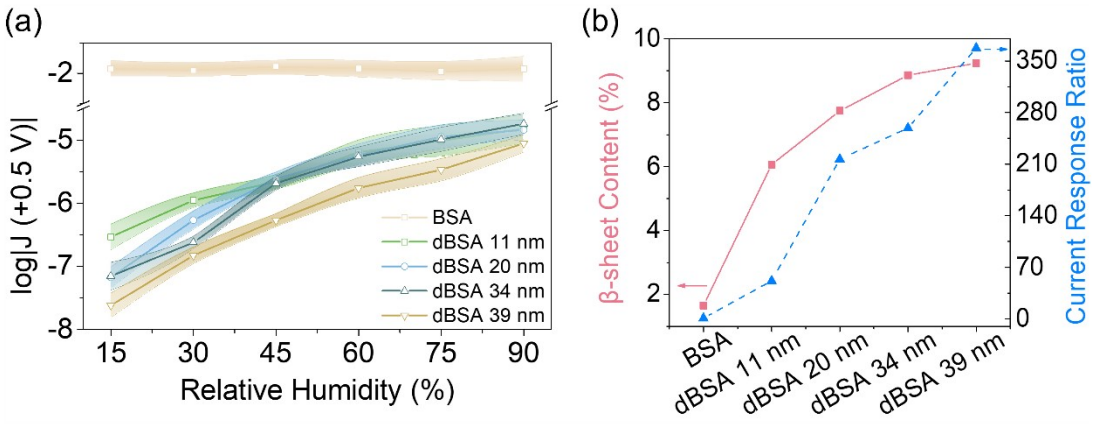

Figure S10. Electrical measurements of BSA monolayer and dBSA nanofilms. (a) Current density of dBSA nanofilms changing with RH at +0.5 V at different thickness and comparing with BSA monolayer. The error bars represent the 95% confidence interval range obtained from Gaussian fitting of at least 380 measurements. (b) Relationship between the β-sheet content and the current response ratio for BSA monolayer and dBSA nanofilms.

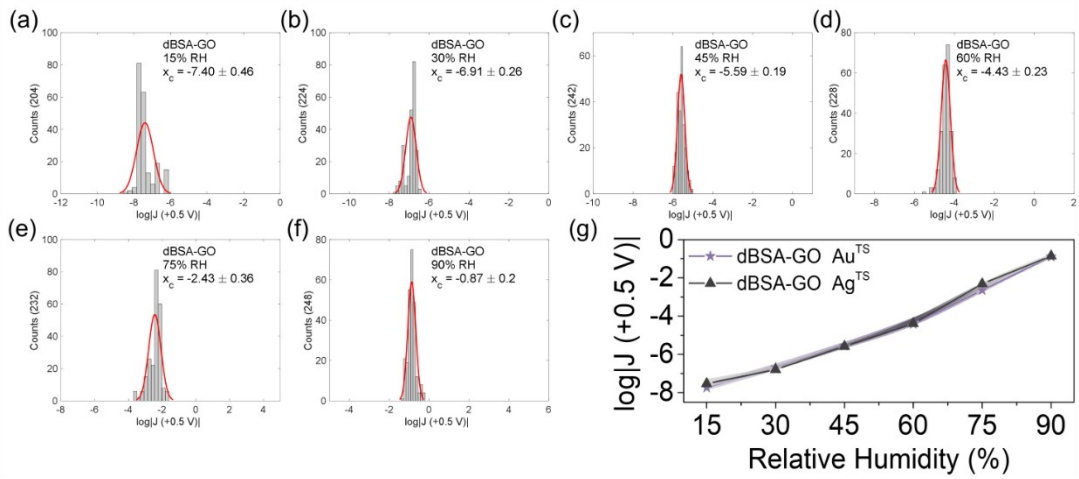

Figure S11. Electrical measurements of dBSA-GO nanofilm. (a-f) Histograms of current density at +0.5 V for dBSA-GO nanofilm junction on Ag^{TS} substrate under RH from 15% to 90% with 15% intervals. (g) Current density of dBSA-GO nanofilm on Au^{TS} and Ag^{TS} substrates changing with RH at +0.5 V. The error bars represent the 95% confidence interval range obtained from Gaussian fitting of at least 200 measurements on Ag^{TS}.

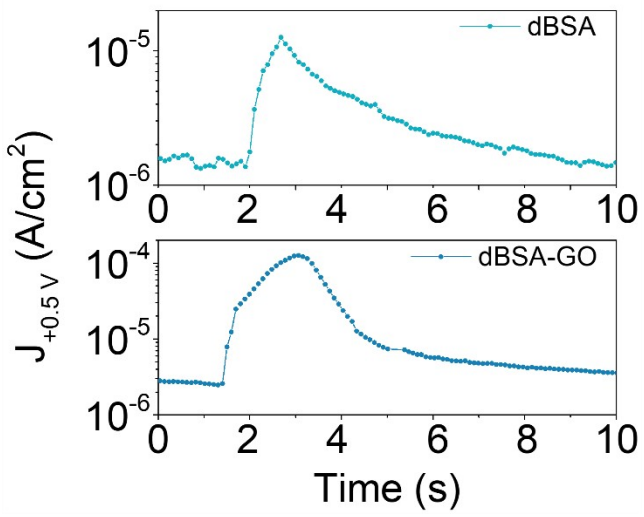

Figure S12. Transient response of dBSA and dBSA-GO nanofilms upon the pulse of H_2O flow (~1 s).

Table S2. Performance comparison of various humidity sensors.

Sensing materials	Sensing principle	Response ratio ($\frac{X_{max}}{X_{min}}$)	Sensing range (RH)	Stability	Response time (s)	Reference
dBSA-GO	Resistance	7.0×10^6	15–90%	3 months	24.4	Our work
GO-PEDOT: PSS-Ag colloids	Resistance	1.03	12–97%	60 min	54	[1]
Pt-nRGO fiber	Resistance	1.0451	6.1–66.4%	/	0.508	[2]
GO	Resistance	~44	35–80%	/	0.030	[3]
GO	Resistance	~45	11–97%	1 month	13	[4]
silk fibroin-rGO	Resistance	1.6	6–97%	34 months	/	[5]
BSA-MoS_2	Resistance	~27	25–85%	/	~1	[6]
BSA-ZnO	Resistance	~120	40–85%	16 days	1.6	[7]
GO	Capacitance	5323.1	10–90%	1 month	15.8	[8]
GO	Capacitance	~21	11–97%	/	25	[9]
GO–PEDOT:PSS	Capacitance	~58	25–85%	/	562	[10]
rGO-$BiVO_4$	Impedance	50	11–95%	2 months	3.6	[11]
rGO	Voltage	2.8	25–85%	/	~1	[12]

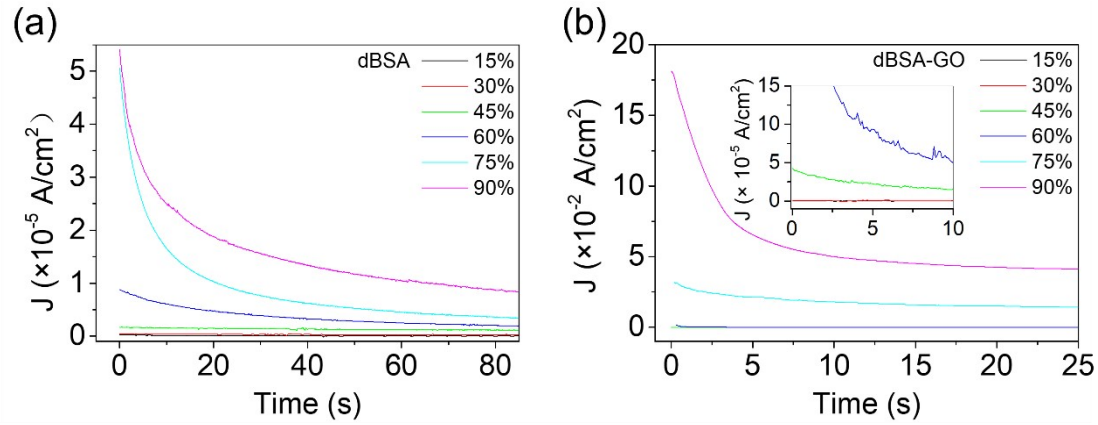

Figure S13. Transient current decay at +0.5 V for (a) dBSA and (b) dBSA-GO nanofilms under RH from 15% to 90% with 15% intervals.

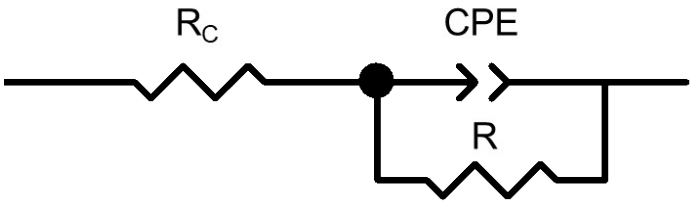

Figure S14. Equivalent circuit for impedance data fitting.

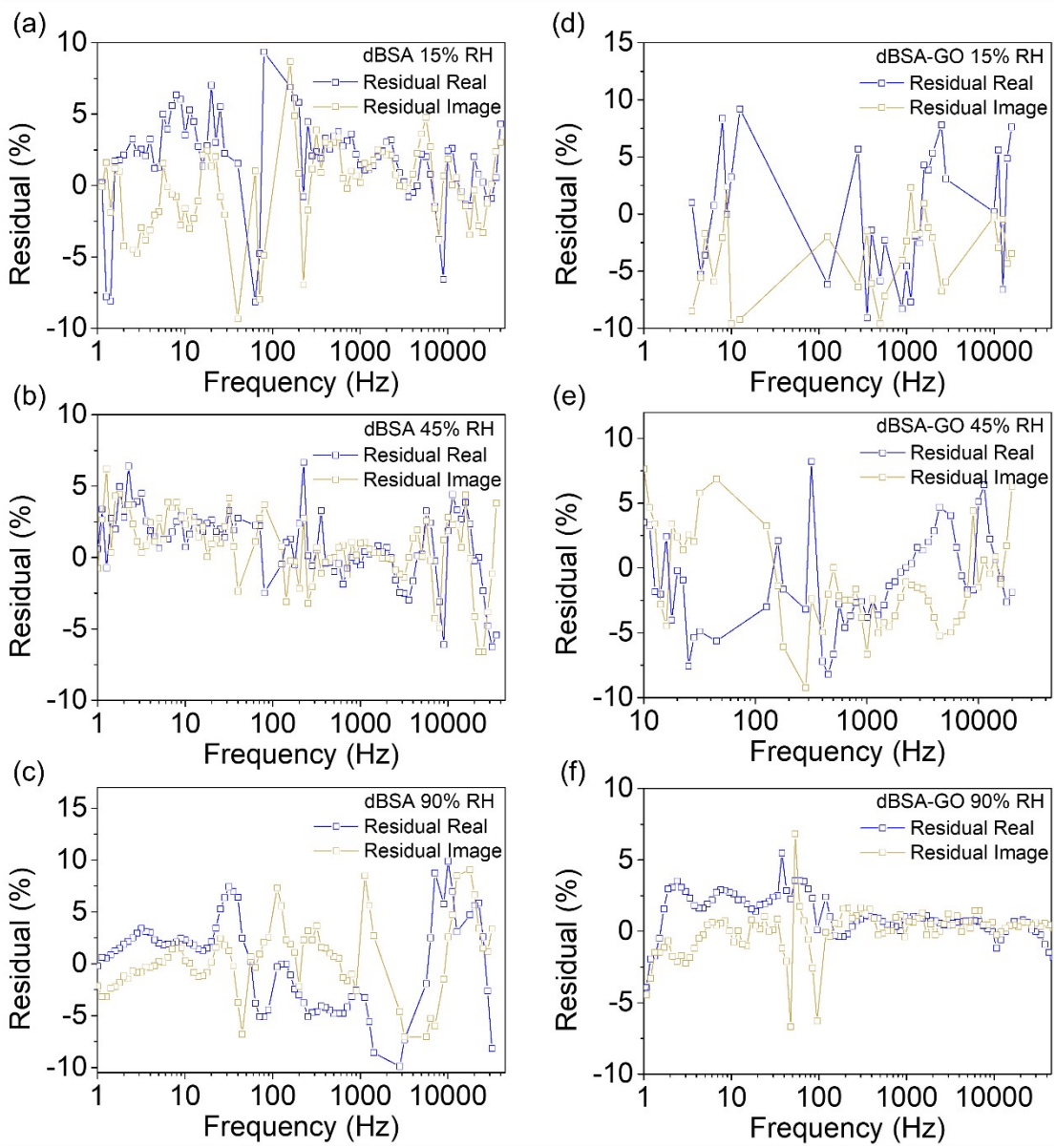

Figure S15. Kramers-Kronig (KK) residual plots for Au^{TS}/nanofilm/GaO_x/EGaIn junctions with (a-c) dBSA and (d-f) dBSA-GO nanofilms at RH of 15%, 45%, and 90%.

The valid impedance spectra should meet the three fundamental requirements, namely linearity, stability, and causality. This means that the impedance signal is derived only from the perturbed voltage of the system, and the system returns to its initial state after removing the perturbed voltage. The KK-test by Lin-KK program can determine whether the system meets these basic requirements.[13-14] The transform formulas are given as

$$Z'(\omega) = \frac{2}{\pi}\int_0^{\infty} \frac{\omega' Z''(\omega')}{(\omega^2 - \omega'^2)} d\omega' \#(2)$$

$$Z''(\omega) = -\frac{2}{\pi}\int_0^{\infty} \frac{\omega Z'(\omega')}{(\omega^2 - \omega'^2)} d\omega' \#(3)$$

where ω is the angular frequency expressed in rad/sec.

Through the KK formulas (Formulas 2-3), predicted *Z'(ω)/Z''(ω)* can be calculated from the measured *Z''(ω)/Z'(ω)*. The residual values between the predicted and experimental results are within 10%, indicating that the data conformed to the KK relationship and were reliable.

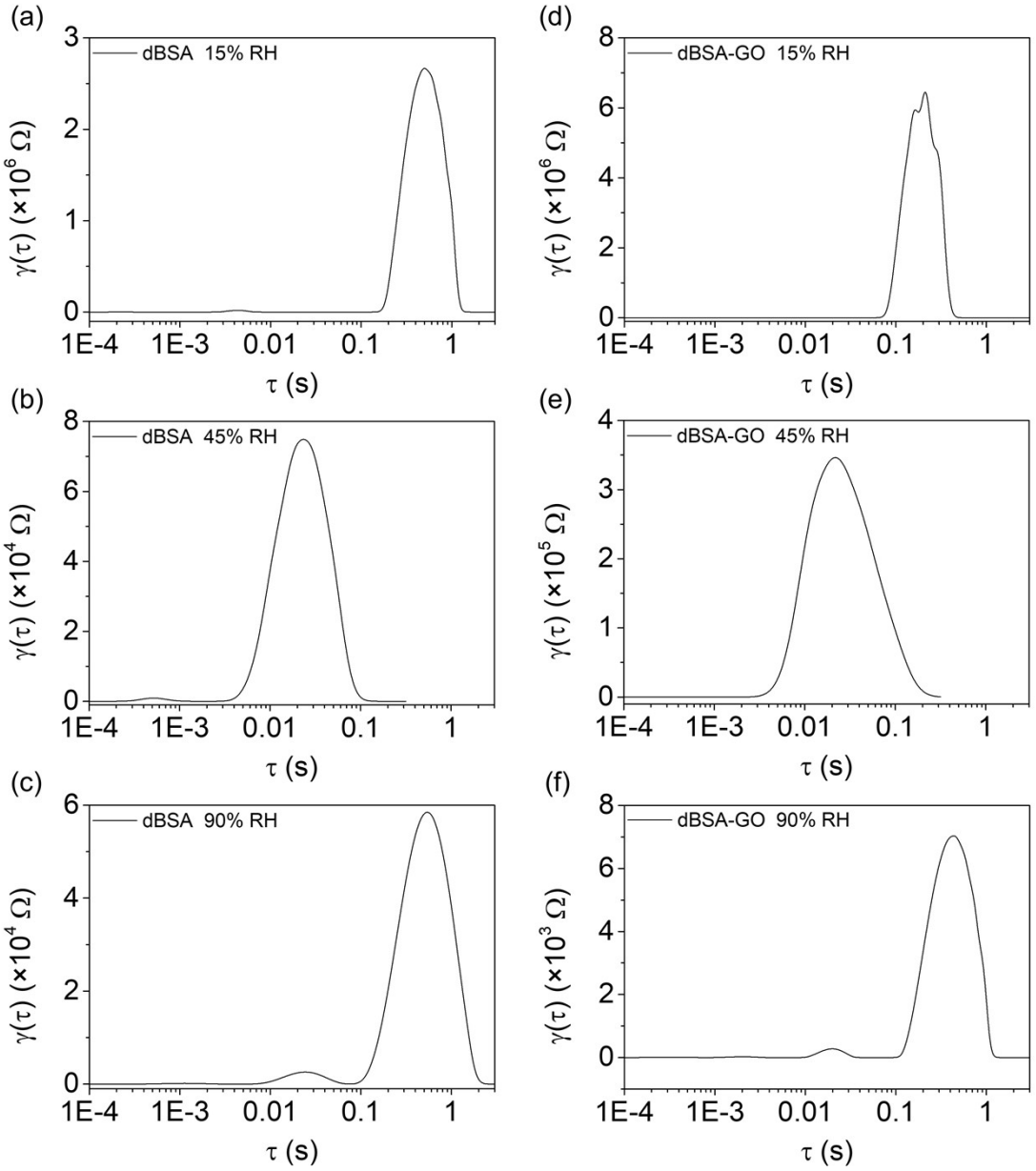

Figure S16. Exact DRT analysis to the impedance results of (a-c) dBSA and (d-f) dBSA-GO nanofilms at RH of 15%, 45%, and 90%.

The DRT is an approach employed to discern the dynamic processes of charge transfer and diffusion in the impedance measurement, enabling the extraction of the characteristic time constants associated with these processes. DRTtools was used to compute the DRT based on Tikhonov regularization with continuous function discretization.[15] Experimental data Z_{exp} measured at the given frequencies were "fitted" with a model Z_{DRT}, which was obtained by the following expression

$$Z_{DRT}(f) = R_{\infty} + \int_{0}^{\infty} \frac{\gamma(\tau)}{1 + i2\pi f\tau} d\tau \#(4)$$

where R_{∞} is the ohmic resistance, and $\gamma(\tau)$ is a suitable distribution function of relaxation times in the system studied.

The presence of only one relaxation time distribution peak in Figure S15 indicated a single electrical process. This result allowed us to establish a reasonable equivalent circuit consisting of one resistor and one capacitor connected in parallel, without any prior assumptions.

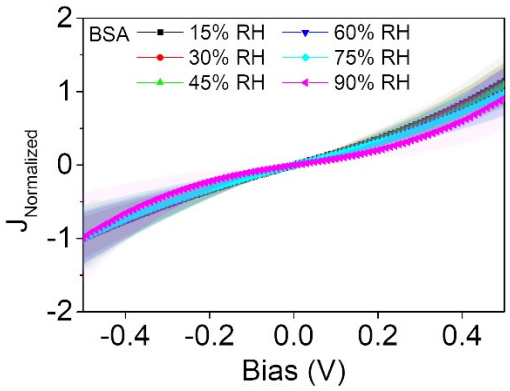

Figure S17. Normalized current density of BSA monolayer vs bias at various RH. The error bars represent the 95% confidence interval range obtained from Gaussian fitting of at least 450 measurements.

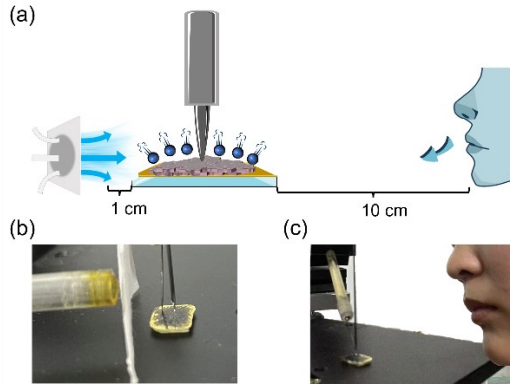

Figure S18. (a) Schematic diagram of humidity sensing. (b) Actual image of contactless simulation of humidity sensing. (c) Actual picture of respiratory monitoring.